Increasing Quantum Limited Sensitivity of Interferometers Using Electromagnetically Induced Transparency

Hunter Rew

Advised by Dr. Eugeniy E. Mikhailov

May 4, 2016

Abstract

We explore the properties of electromagnetically induced transparency (EIT) and its applications as a frequency filter in the field of gravitational wave interferometry. Through modeling and simulation, we determine parameters for atom-light configurations of multi-state atoms which will theoretically allow for transmission frequencies and intensities of squeezed light in a range suitable for increasing sensitiviy levels in gravitational wave interferometers. This corresponds to contrasts greater than 50% and linewidths of 100 Hz or less. We produce EIT experimentally and characterize the distributions by fitting them to a generalized Lorentzian. The largest contrast observed is 3.9% with a linewidth of 657 Hz. The smallest linewidth observed is 202 Hz with a contrast of 0.84%.

Acknowledgments

I would like to thank Dr. Eugeniy Mikhailov and Dr. Irina Novikova, both of whom have been mentors to me since the beginning of my studies at William & Mary. Without their guidance and thoughtfulness, I would never have received the opportunities that I did. I would also like to thank Dr. Ji Mun of Thomas Nelson Community College for always encouraging me to follow my passions, regardless of the feasibility.

Contents

List of Figures

Introduction

1.1 Gravitational wave interferometers

A prediction of the general theory of relativity is that moving objects produce waves in spacetime which propagate in all directions at the speed of light. These gravitational waves (GWs) contract space in one dimension while expanding space in transverse dimensions, alternating with each half period. Attempts to confirm the existence of GWs have resulted in the construction of high precision laser interferometers across the Earth [1]. These interferometers use mirrors as test masses so that as a GW passes through, one arm will shorten while the other elongates, causing a measurable phase shift of the light. A simplified diagram of one of these interferometers is shown in Figure 1.1.

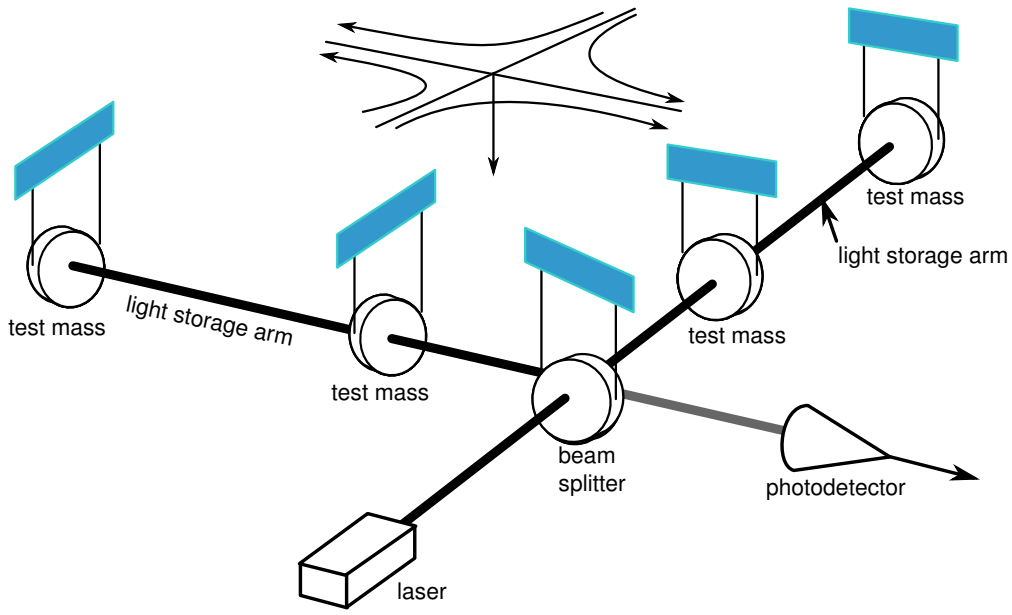

Figure 1.1: The Laser Interferometer Gravitional Wave Observatory (LIGO) is a Michelson interferometer with 4 km long Fabry-Perot cavities as arms. LIGO has 2 sites 3000 km apart in Livingston, Louisiana and Hanford, Washington.

1.2 Squeezed states and their application to interferometry

The uncertainty principle places a fundamental limit on how precisely two quadratures, such as position and momentum, can be known. A generic form of this limit is shown in Equation 1.1, where χ_1 and χ_2 are the measurable quadratures.

$$\Delta\chi_1 \Delta\chi_2 \geq Limit \tag{1.1}$$

Due to the Heisenberg uncertainty principle, the amplitude and phase of light cannot be known beyond a quantum limited precision. This uncertainty in a measurement can be visualized as Figure 1.2, where rather than a distinct point measurement, there is a "ball" of uncertainty in the phase-amplitude plane. The area of this ball is governed by the uncertainty principle, however, there is no law that these uncertainties must be symmetric [1]. For example, the ball could be squeezed into an ellipse at some angle (as shown in Figure 1.2) so that, while maintaining the same total area, the uncertainty in amplitude becomes much larger than the uncertainty in phase. This is analogous to purposefully losing information of the amplitude (increasing its uncertainty), so that the phase can be known with greater precision while still satisfying the uncertainty principle. Once this is done, the light is said to be in a squeezed state. Using squeezed light, an interferometer can measure the signal of interest beyond the standard quantum limit, thereby increasing sensitivity to GWs [1]. This would enable GW observatories such as LIGO to make detections more frequently from a broader range of astronomical sources. However, LIGOs optical fields are already in a squeezed state due to radiation pressure noise within the Fabry-Perot cavities [2]. In order to inject a new squeezed state, the squeeze angle must be matched [1, 2]. This necessitates the use of an optical filter with a linewidth < 100 Hz [1, 2]. In addition to the requirement of a narrow linewidth, a filter is of little use if the resulting signal cannot be measured. In

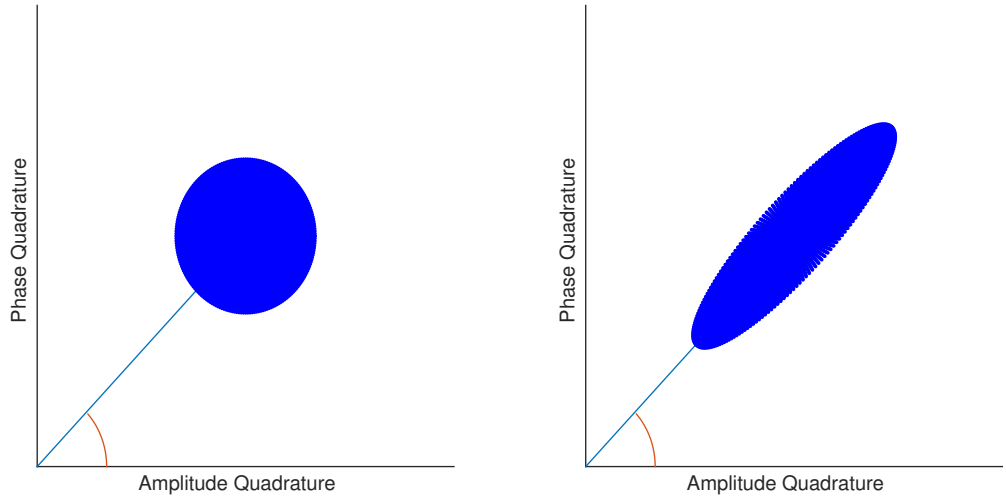

Figure 1.2: The left plot shows a symmetric "ball" of uncertainty. The right plot shows the uncertainty squeezed.

general, a good filter should provide contrast of at least 50% and peak transmission of at least 95%.

1.3 Electromagnetically induced transparency as a frequency filter

One option for a frequency filter, which is suitable for LIGO, is Electromagnetically Induced Transparency (EIT). EIT is the phenomenon of an opaque material becoming transparent for certain frequencies of light. This occurs by "pumping" atoms into a "dark" state by applying optical fields which match the frequency difference between excited states and the hyperfine ground states, creating a superposition of the ground states which doesn't interact with the applied fields [3]. This allows a "probe" to pass through the medium with high transmission across a slim range of frequencies. An EIT media could potentially be used as a filter for rotating the angle of an injected squeezed state [2]. EIT has been shown to produce linewidths narrower than 100 Hz, while maintaining low optical losses and high contrast [2]. Beyond these requirements, an EIT filter also offers the convenience of being tuned electronically.

Theory

2.1 The lambda model

The Λ model is a simplistic atomic configuration consisting of 3 states in total, 2 ground states and 1 excited state. A representation of the model and the optical fields that are applied is shown in Figure 2.1. Δ is the 1-photon detuning, δ is the 2-photon detuning, γ is the decay rate from the excited state, $|a\rangle$, to the hyperfine ground states, $|b\rangle$ and $|c\rangle$, and γ_{bc} is the decay rate between ground states. Ω_d and Ω_p are the Rabi frequencies of the fields applied at transitions $|c\rangle \longrightarrow |a\rangle$ and $|b\rangle \longrightarrow |a\rangle$, respectively. These are measures of how strongly coupled the light fields are to the transitions which they are applied. Rabi frequencies are defined as:

$$\Omega = \frac{d_{i,j}E}{\hbar} \tag{2.1}$$

where $d_{i,j}$ is the dipole moment between states $|i\rangle$ and $|j\rangle$ and E is the light amplitude field.

The populations and coherences evolution is given by the equations below [4]:

$$\dot{\rho}_{aa} = -i\Omega_p^*\rho_{ab} + i\Omega_p\rho_{ba} - i\Omega_d^*\rho_{ac} + i\Omega_d\rho_{ca} - 2\gamma\rho_{aa} \tag{2.2}$$

$$\dot{\rho}_{bb} = i\Omega_p^*\rho_{ab} - i\Omega_p\rho_{ba} + \gamma\rho_{aa} - \gamma_{bc}\rho_{bb} + \gamma_{bc}\rho_{cc} \tag{2.3}$$

$$\dot{\rho}_{cc} = i\Omega_d^*\rho_{ac} - i\Omega_d\rho_{ca} + \gamma\rho_{aa} - \gamma_{bc}\rho_{cc} + \gamma_{bc}\rho_{bb} \tag{2.4}$$

$$\dot{\rho}_{ab} = -\Gamma_{ab}\rho_{ab} + i\Omega_p(\rho_{bb} - \rho_{aa}) + i\Omega_d\rho_{cb} \tag{2.5}$$

$$\dot{\rho}_{ca} = -\Gamma_{ca}\rho_{ca} + i\Omega_d^*(\rho_{aa} - \rho_{cc}) - i\Omega_p^*\rho_{cb} \tag{2.6}$$

$$\dot{\rho}_{cb} = -\Gamma_{cb}\rho_{cb} - i\Omega_p\rho_{ca} + i\Omega_d^*\rho_{ab} \tag{2.7}$$

where the coherence decay rate Γ_{ij} is given by Equations 2.8 through 2.10 [4].

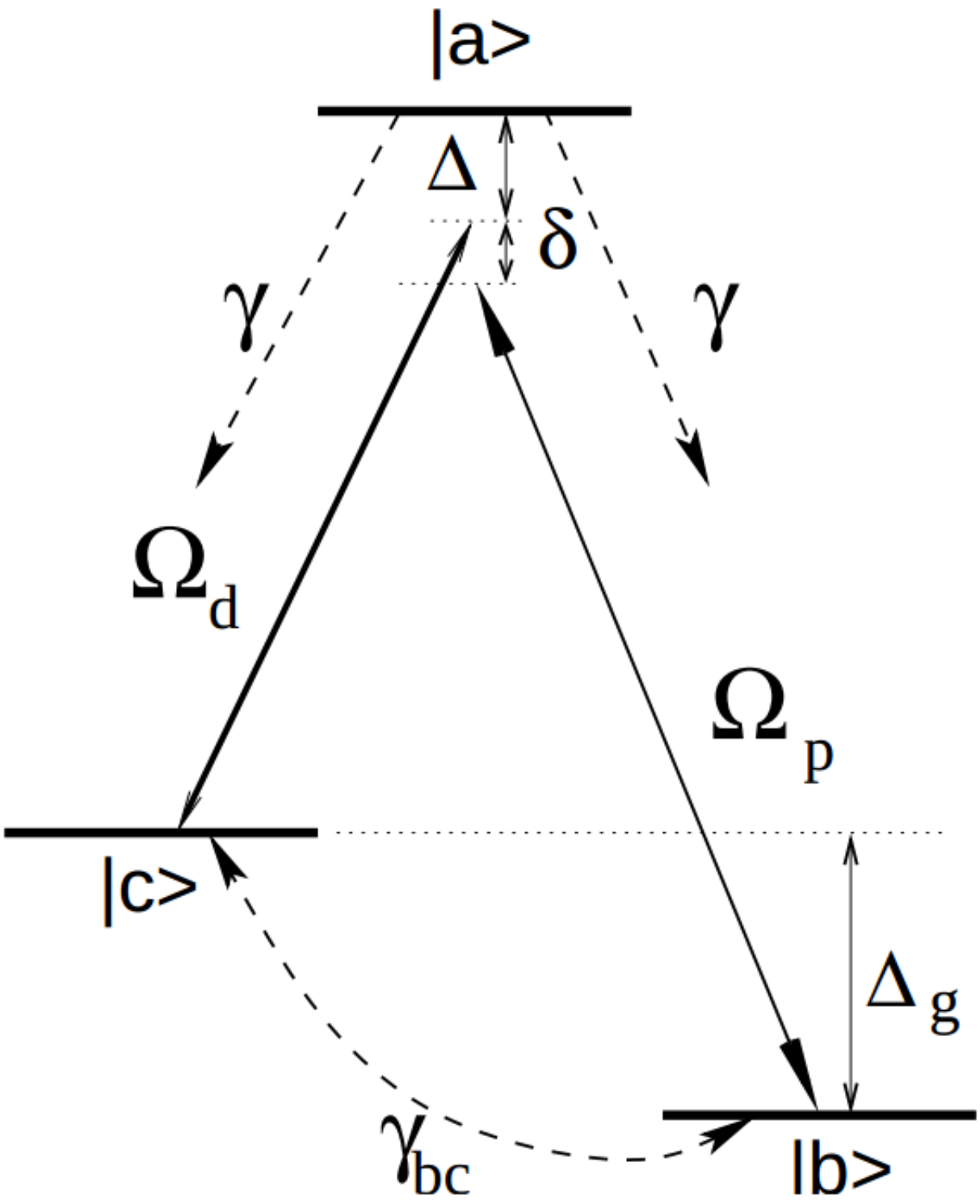

Figure 2.1: Λ configuration [4]

$$\Gamma_{ab} = \gamma + i(\Delta + \delta) \tag{2.8}$$

$$\Gamma_{ca} = \gamma - i\Delta \tag{2.9}$$

$$\Gamma_{cb} = \gamma_{bc} + i\delta \tag{2.10}$$

Because the density matrix is Hermitian, the remaining off diagonal elements can be found as:

$$\rho_{ij} = \rho_{ji}^{*}, i \neq j \tag{2.11}$$

2.2 The dark state in a 3-state atom

In order for EIT to be realized, there must be a state for an atom in which absorption of light does not occur. For this to be possible, the population of the excited state, described in Equations 2.2 to 2.7, must be zero. This means that the wave function describing this system must be a superposition of only the ground states. Such a state occurs when the frequency difference of the applied fields is equal to the hyperfine splitting of the ground states. This condition is called a 2 photon resonance and results in the wave function given in Equation 2.12, known as the dark state [3].

$$|D\rangle = \frac{\Omega_d e^{-i\omega_b t}|b\rangle - \Omega_p e^{-i\omega_c t}|c\rangle}{\sqrt{\Omega_p^2 + \Omega_d^2}} \tag{2.12}$$

Here ω_b and ω_c are the frequencies of states $|b\rangle$ and $|c\rangle$, respectively. Atoms are pumped into the dark state by Ω_d, the drive field. While there, atoms no longer transition to the excited state. This enables Ω_p, the probe field, to pass through without absorption. The dark state deteriorates as the fields are detuned from the two photon resonance, giving the EIT an inherent linewidth [3]. An approximation of this linewidth, γ_{EIT}, is given below [4].

$$\gamma_{EIT} = \gamma_{bc} + \frac{|\Omega_d|^2 + |\Omega_p|^2}{\gamma} \tag{2.13}$$

Simulation

3.1 Simulation methods and parameters

In order to see the evolution of the light-atom system, we used numerical integration software called eXtensible Multi-Dimensional Simulator (XMDS). This allowed for integrating Equations 2.2 through 2.7 across time while varying the detuning to see how the dark state changed with respect to the probe frequency and propagation through a medium. Attaining high resolution in detuning and propagation quickly increases the memory requirements of the simulation, so it was necessary to utilize William and Mary's high performance computing cluster, SciClone.

Simulations were run with the following parameters:

- Drive Rabi frequency (Ω_d): varied from 16.6 to 25.0 kHz
- Probe Rabi frequency (Ω_p): 0.1 Hz
- Excited state decay (γ): 6 MHz
- Ground state decay (γ_{bc}): 1 Hz
- Length of medium: varied from 0 to 2 cm
- Particle density of medium (N): 1×10^{15} particles per m^3

Equation 3.1 is used in simulations to account for the evolution of the drive and probe fields with propagation [4]. Wave vector $k = 2\pi/\lambda$, where wavelength $\lambda = 794.7nm$.

$$\frac{\partial E}{\partial z} + \frac{1}{c}\frac{\partial E}{\partial t} = 2\pi i k N \sum_{i,j} d_{i,j}\tilde{\rho}_{i,j} \tag{3.1}$$

3.2 Simulation results and analysis

Because EIT does not have precisely 100% transmission, a small percentage of the probe intensity is lost to atoms while propagating. When the probe is detuned from the resonant frequency, however, transmission drops considerably more, resulting in the development of transmission resonance with characteristic contrast and linewidth (Figure 3.1). These are the properties which are measured for any EIT from specific parameters.

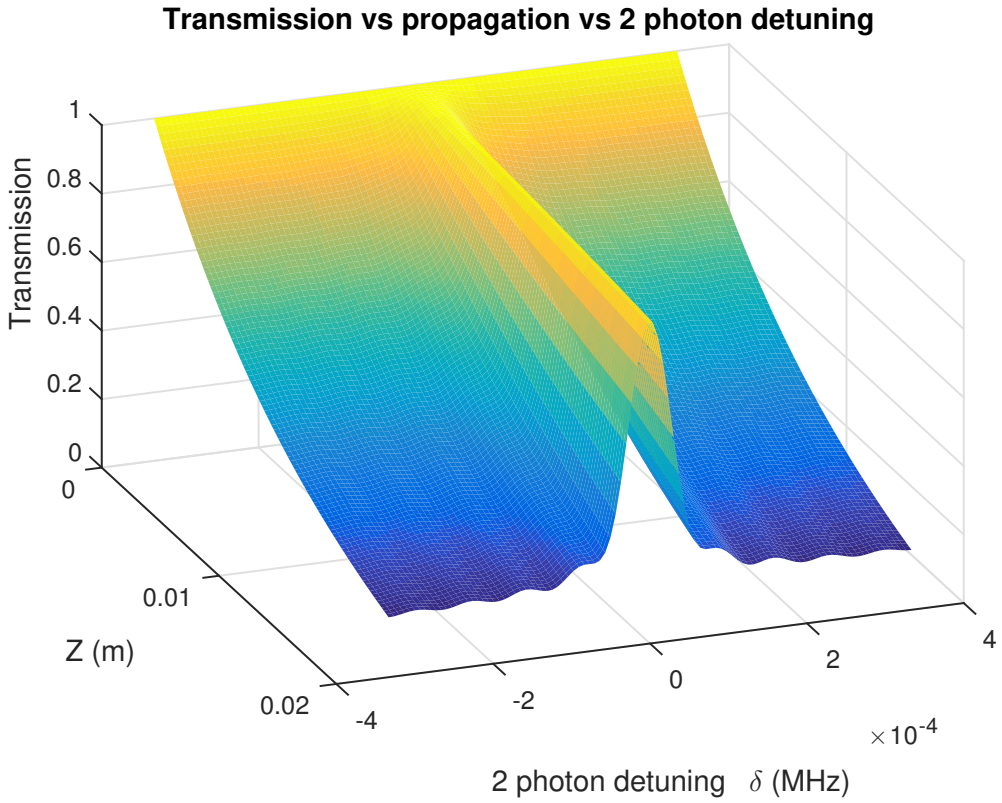

Figure 3.1: The evolution of EIT as it propagates through an atomic medium in the Z direction. With increasing atom interactions, the field is absorbed for frequencies far from resonance, while frequencies near resonance are free to pass.

In order to accurately determine the linewidth and contrast, we fit these lineshapes to a generalized Lorenztian as given in [5].

$$Transmission = A\frac{\gamma_r^2}{\gamma_r^2 + \delta^2} + B\frac{\gamma_r \delta}{\gamma_r^2 + \delta^2} + C \tag{3.2}$$

Here the term with coefficient A is the absorptive Lorentzian and the B term is the dispersive Lorentzian. Parameters A, γ_r, and δ are the contrast, half width half maximum (HWHM), and 2 photon detuning, respectively [5]. An example of this curve fitted to simulation data is shown in Figure 3.2.

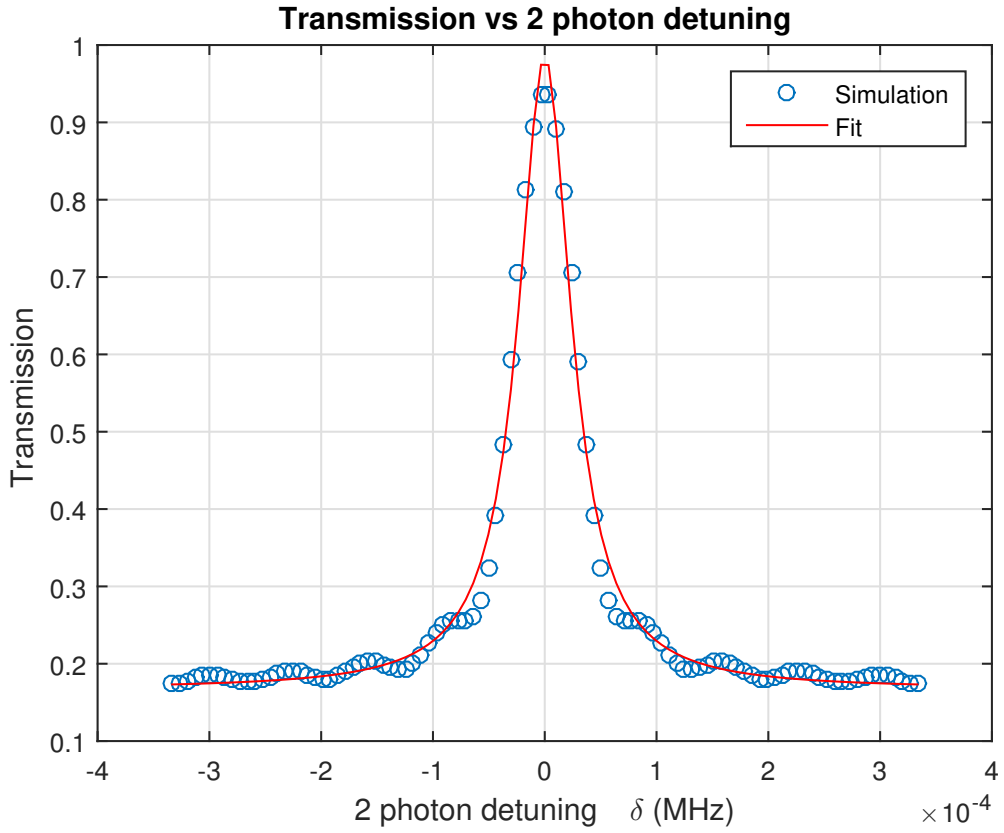

Figure 3.2: An example EIT transmission distribution fitted to a Lorentzian.

The effects of initial drive power (Ω_d) and propagation length (z) on transmission are displayed in Figure 3.3. This shows that transmission increases with drive and decreases with propagation. From Figure 3.4 one can see that contrast does indeed increase with propagation. This also results in a narrowing of the linewidth with propagation, as shown in Figure 3.5. Given that an ideal filter should have high transmission and contrast with a narrow linewidth, one can see that these 3 measures compete with one another in terms of their respective ideal parameters. For instance, linewidth is improved with propagation, while transmission is reduced. Using Figure 3.6 we can see that the requirement of a linewidth

< 100 Hz can be achieved with contrast $> 50\%$ while maintaining high transmission ($> 95\%$). This area includes drives ranging from 17 kHz to at least 25 kHz for nearly any medium length greater than 1 cm. This is the range that is useful for applications of EIT as a frequency filter in GW interferometers.

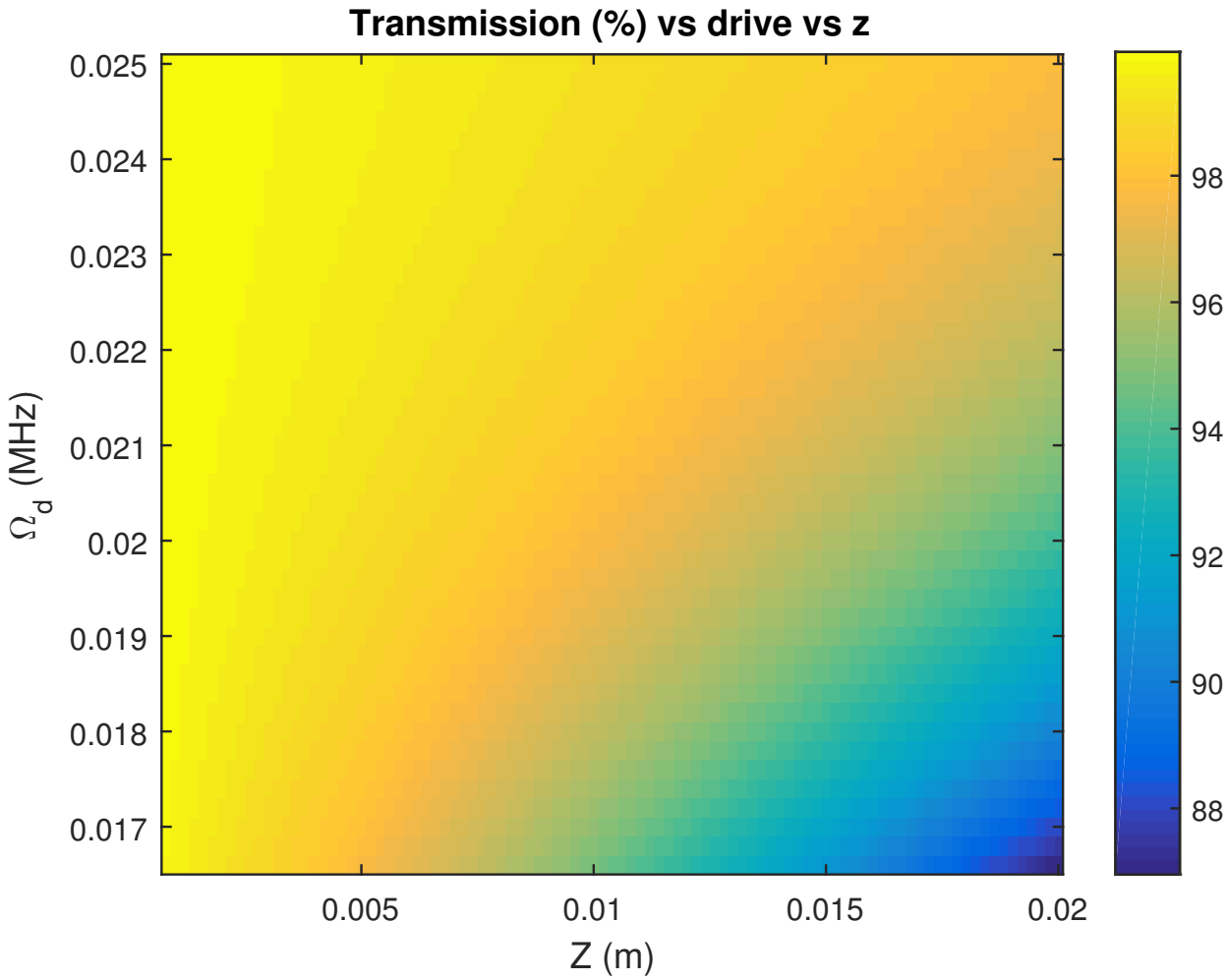

Figure 3.3: This map shows how the transmission of the EIT is affected by the drive Rabi frequency (Ω_d) and length (Z) of the atomic media through which the fields are propagating.

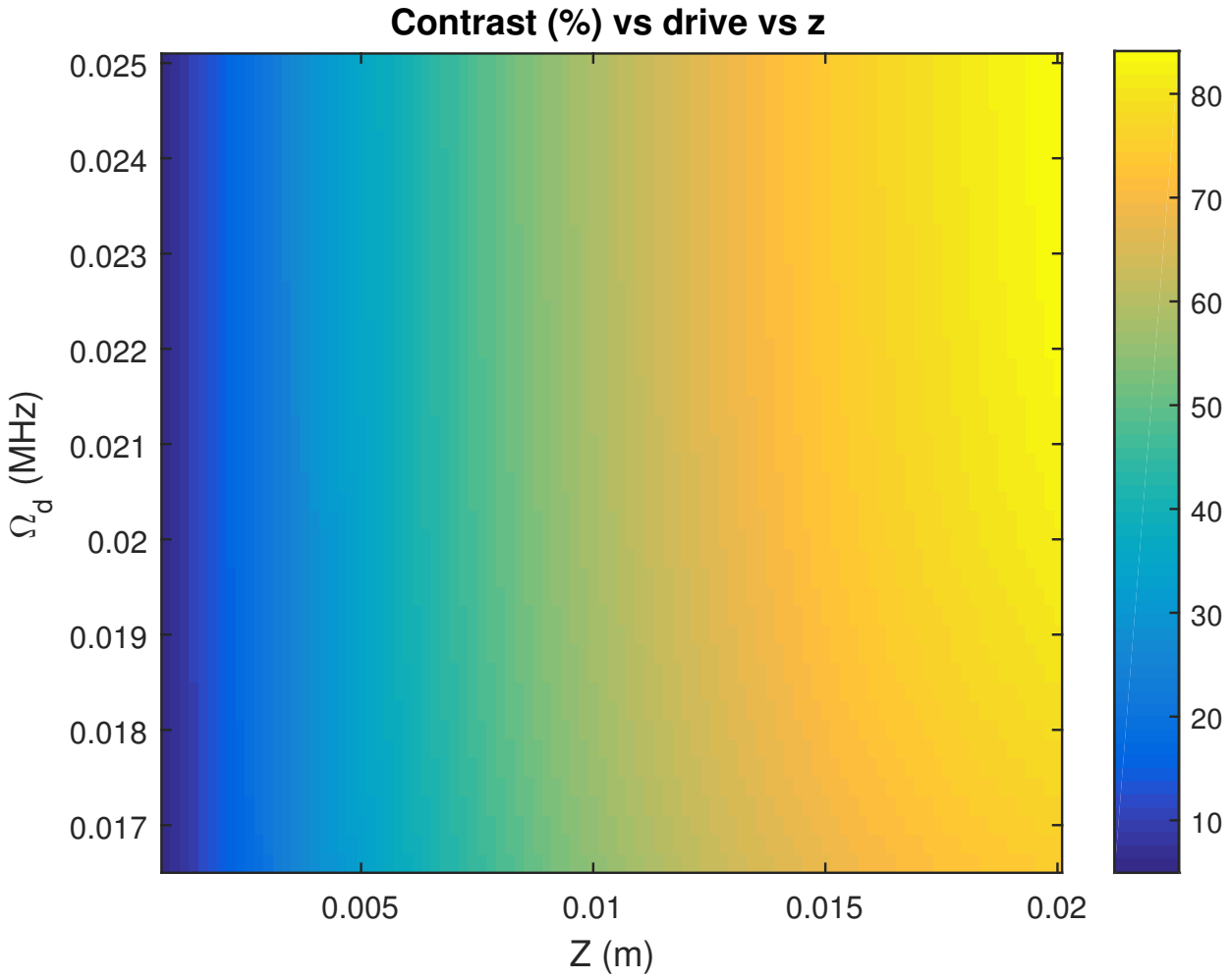

Figure 3.4: This map shows how the contrast of the EIT is affected by the drive Rabi frequency (Ω_d) and length (Z) of the atomic media through which the fields are propagating.

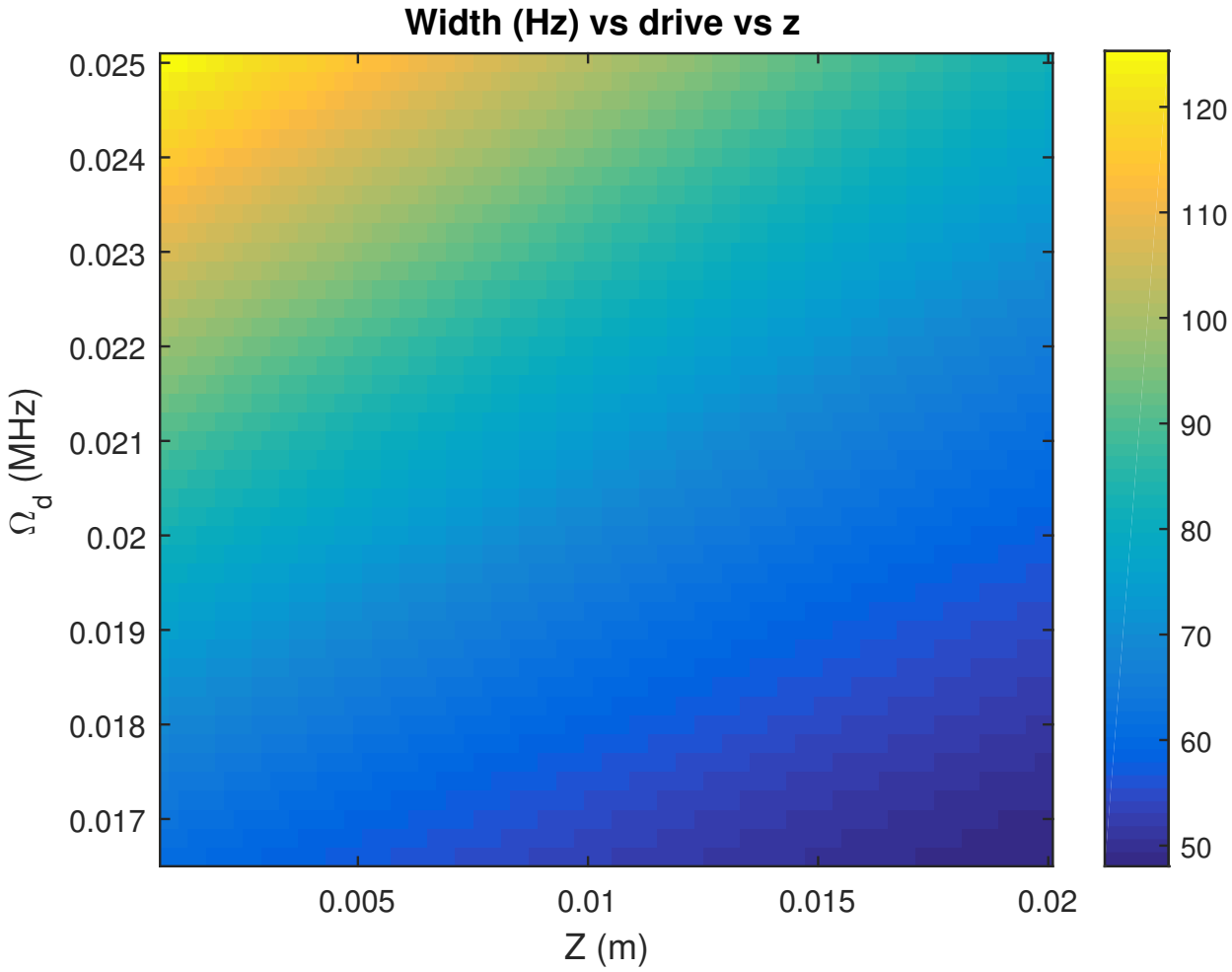

Figure 3.5: This map shows how the linewidth of the EIT is affected by the drive Rabi frequency (Ω_d) and length (Z) of the atomic media through which the fields are propagating.

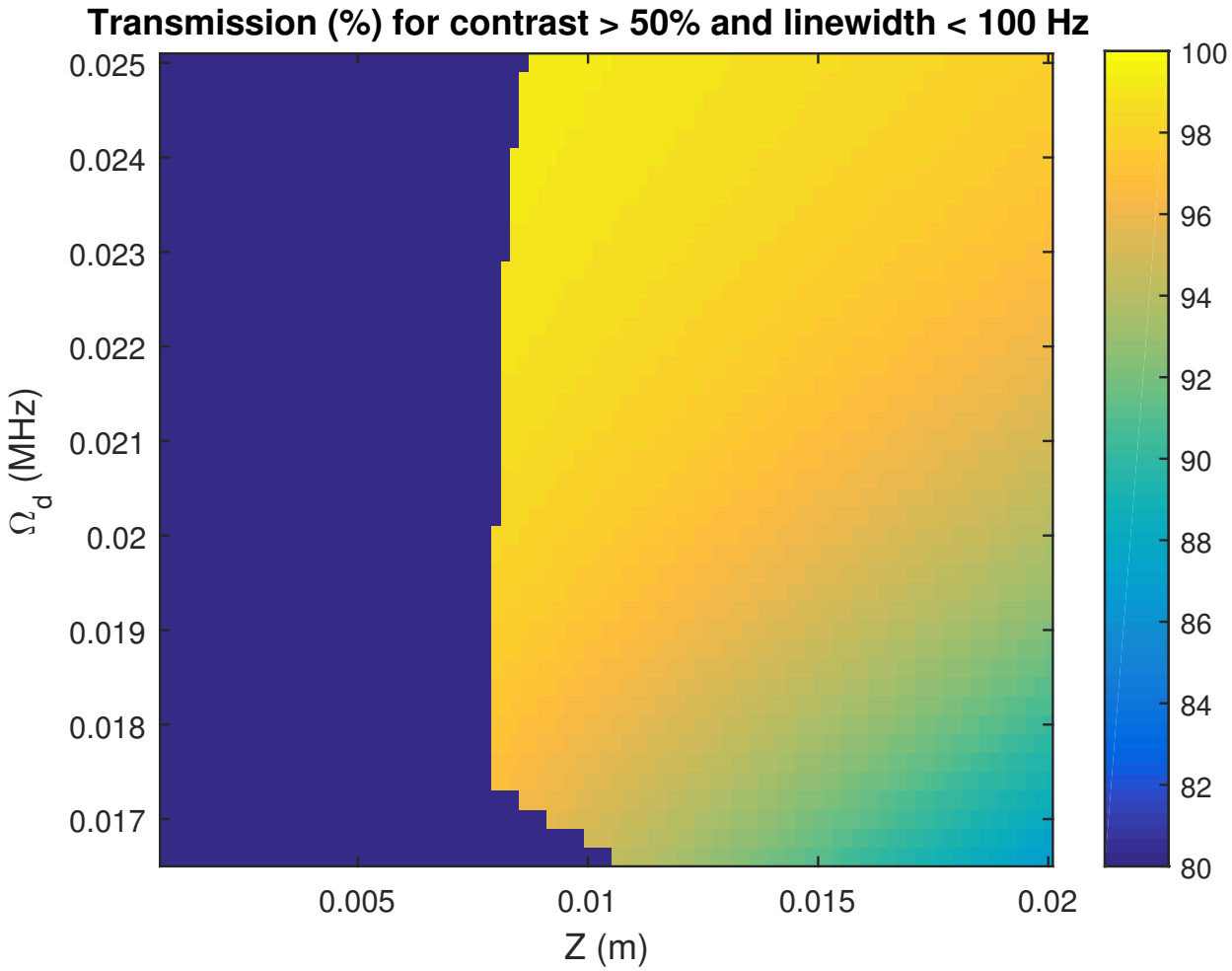

Figure 3.6: This map shows transmission for the regions of drive and z where contrast is > 50% and linewidth < 100 Hz.

Experiment

4.1 Experimental setup and procedures

4.1.1 Setup

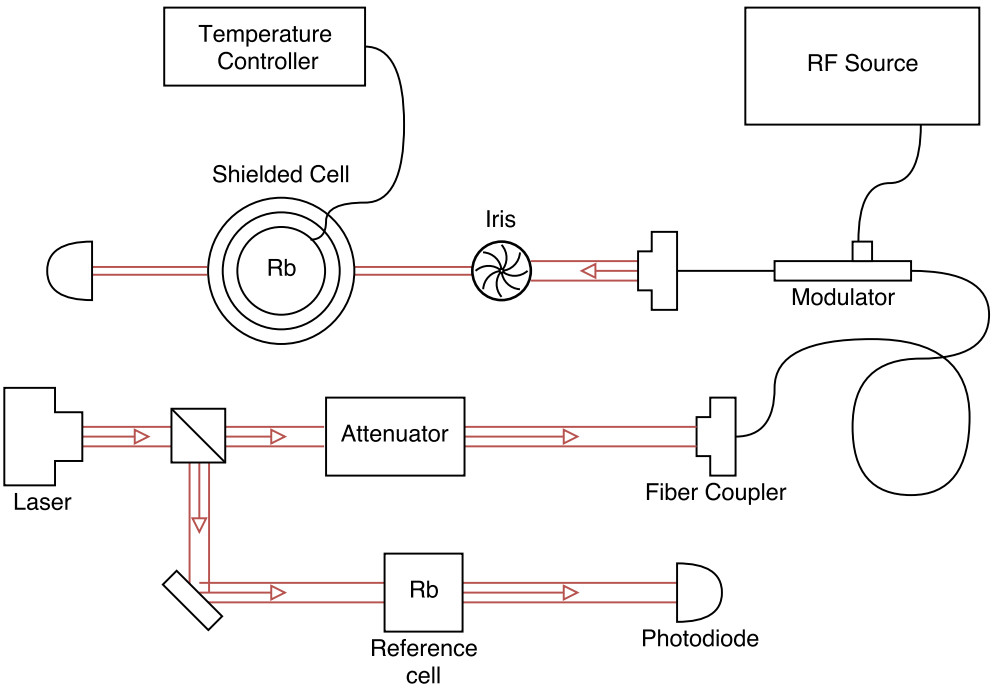

Figure 4.1: A diagram of the experiment configuration.

Figure 4.1 shows a schematic of our experimental setup. We begin with a semiconductor laser tuned to the $5S_{\frac{1}{2}}\ F = 2 \longrightarrow 5P_{\frac{1}{2}}\ F = 1$ transition frequency of ^{87}Rb using the reference cell. The beam is then attenuated before being passed to an electro-optic modulator (EOM). The EOM is modulated at a frequency of 6.834 GHz, corresponding to the hyperfine splitting of ^{87}Rb. This creates a side band with the main beam, to act as our probe and drive fields, respectively. The probe is swept through a range of 4.768 kHz over a time of 101 ms. The two fields then pass through a magnetically shielded cell of ^{87}Rb before reaching a photodiode. The cell is roughly 1.5 cm in diameter and 1 cm in length. It has a high temperature anti-relaxation coating intended to extend the lifetime of the dark state (decrease γ_{bc} in Equation

2.13), and so allow for narrower linewidths. Cell temperature is controlled using a heating element and thermocouple connected to an external controller.

4.1.2 Procedures for varying beam intensity

It is important to understand the dependence of linewidth, contrast, and transmission on intensity in order to determine ideal experimental parameters. Measurements with varying intensity are done by changing the attenuation of the beam before the cell through the addition of neutral density filters. The resulting power is measured. This measurement is what is used for most of our plots, however, this can be converted to a Rabi frequency as below [4].

$$\Omega = 2\pi\gamma\sqrt{\frac{I}{8}} \tag{4.1}$$

Here intensity, I, is measured in $\frac{mW}{cm^2}$. For ^{87}Rb, γ is 6 MHz. The power measured is a roughly equal combination of the drive field and two probes (the EOM produces two sidebands at $\pm$ the modulation frequency). This estimates our drive and probe Rabi frequencies to be in the range of 5 to 30 MHz. This is much larger than the regime which simulations cover, as with our current setup it would not be feasible to detect such small fields.

4.1.3 Procedures for varying cell density

As with varying power, we also need to know the dependence of EIT properties on density. Rather than increasing atom-light interactions through lengthening the cell as we did in simulations, experimentally it is easier to increase the density of atoms in the cell. This is done by increasing the temperature. When taking any measurements with varying temperature, we set temperature first, then iterate through any secondary variables such as power or beam size. This is due to the prolonged amount of time required for the temperature to become stable at a new point. We have taken measurements for temperatures ranging from 60 to 75 degrees Celsius in increments of 5 degrees. This corresponds to a range in particle

concentration of about 1×10^{11} to 9×10^{11} ($\frac{particles}{cm^3}$) [6].

4.1.4 Procedures for varying beam waist

Although it was not addressed in our simulations, studies with anti-relaxation coated cells have shown that a smaller beam waist results in a finer linewidth of the EIT resonance [7]. In order to incorporate this variable into our study, an iris was placed in front of the Rb cell as shown in Figure 4.1. Rather than attempting sub-millimeter measurements of the beam waist, we quantify the waist size by the percentage of power passed through the iris. These measurements are then converted to a fraction of our beams ω_0, the radius at which intensity has dropped by a factor of e^2. We have taken data for 3 beam waist values: full beam, $1.2\omega_0$, and $0.8\omega_0$, corresponding to roughly 100, 50, and 25 percent of the full beam power, respectively.

4.2 Experimental data and data analysis

4.2.1 Contrast and linewidth vs power for varying particle concentration

As with simulations, we measure the linewidth and contrast of the experimental EIT lineshapes by fitting them to the generalized Lorentzian given in Equation 3.2. An example of this curve fitted to experimental data is shown in Figure 4.2.

The data collected as described in Section 4.1.3 is shown on the following pages. Figures 4.3 through 4.12 show trends of contrast, linewidth, and transmission as functions of drive field power and rubidium concentration alongside simulation trends for comparison. The simulation trends are taken as slices from the figures in Section 3.2. Trends where drive Rabi frequency (Ω_d) is the independent variable are given in terms of Ω_d^2 in order to be comparable to experimental trends where power is directly measured (see Equation 4.1 for

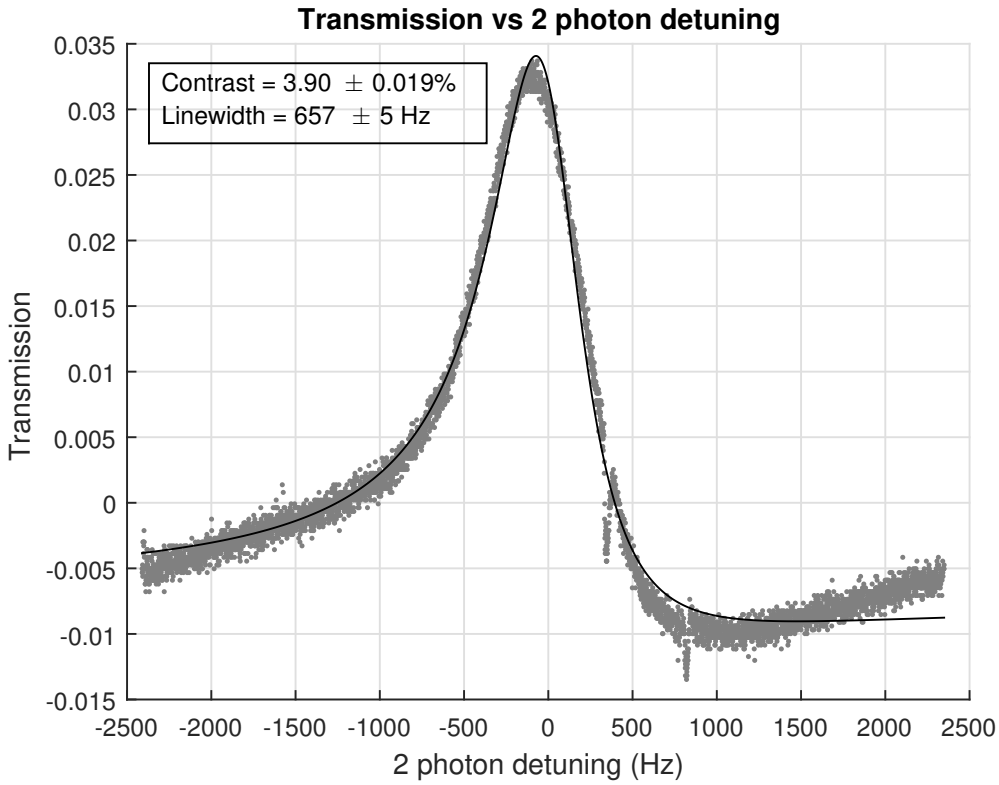

Figure 4.2: Fit of experimental EIT with a contrast of 3.9% and linewidth of 657 Hz. Error bars given represent a 95% confidence interval.

Rabi frequency's relation to power).

We see that contrast increases with drive power, as well as a pattern of contrast increasing with density. Both of these results were also observed in simulations (Figures 3.4, 4.3, and 4.9), with the exception that in experiment we see contrast eventually declines with increasing power and concentration rather than plateauing (Figures 4.4 and 4.10). Linewidth clearly increases with power. This experimental trend is expected from the simulation results in Figures 3.5 and 4.5.

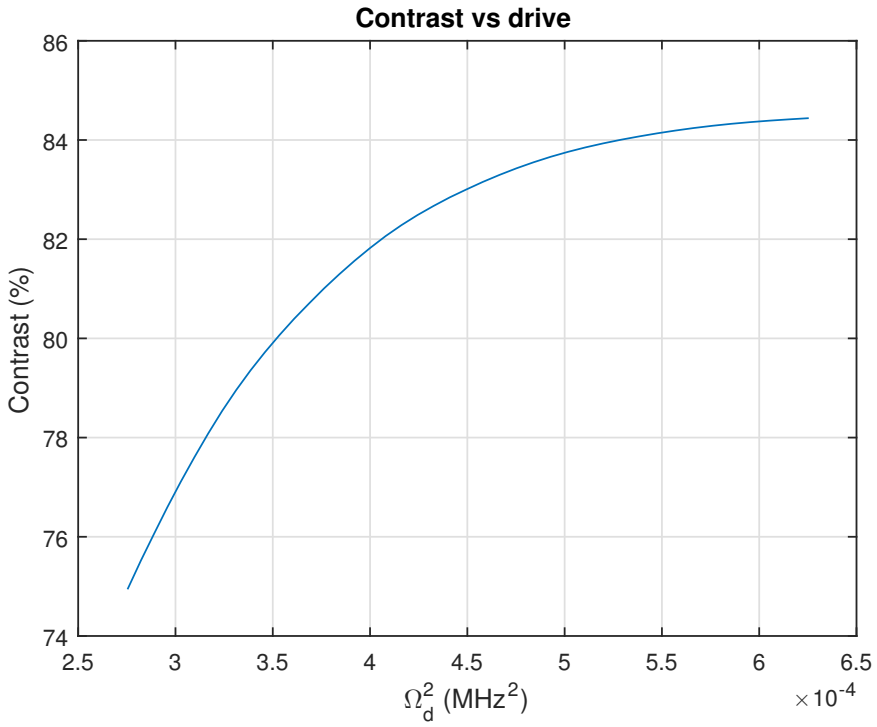

Figure 4.3: Simulation results of contrast vs power (measured in Rabi frequency)

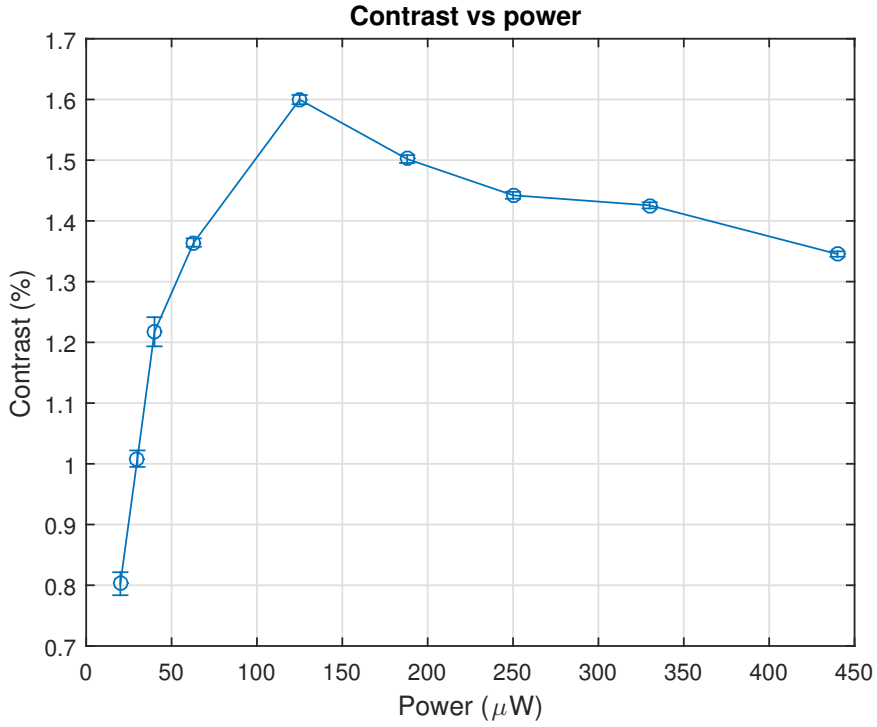

Figure 4.4: Experimental results of contrast vs power. Beam size is $0.8\omega_0$ and particle concentration is 6.3×10^{11} (1/cc).

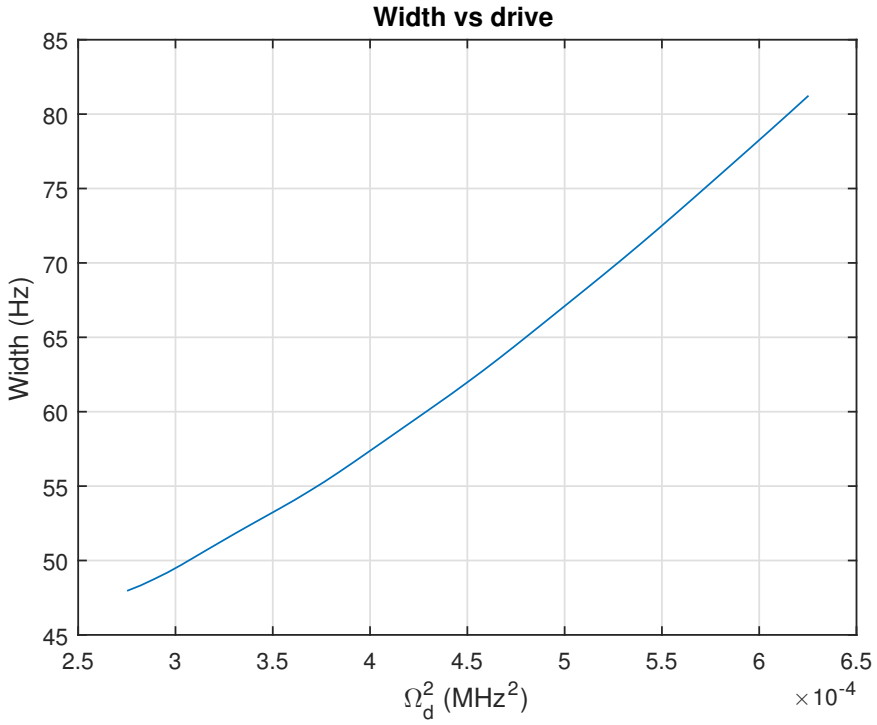

Figure 4.5: Simulation results of linewidth vs power (measured in Rabi frequency)

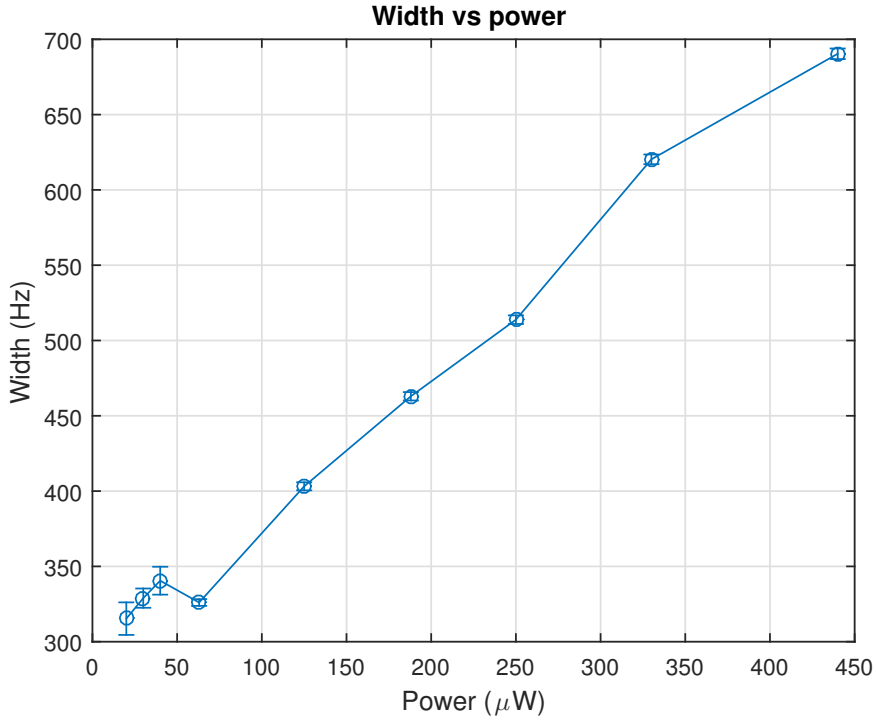

Figure 4.6: Experimental results of linewidth vs power. Beam size is $0.8\omega_0$ and particle concentration is 6.3×10^{11} (1/cc).

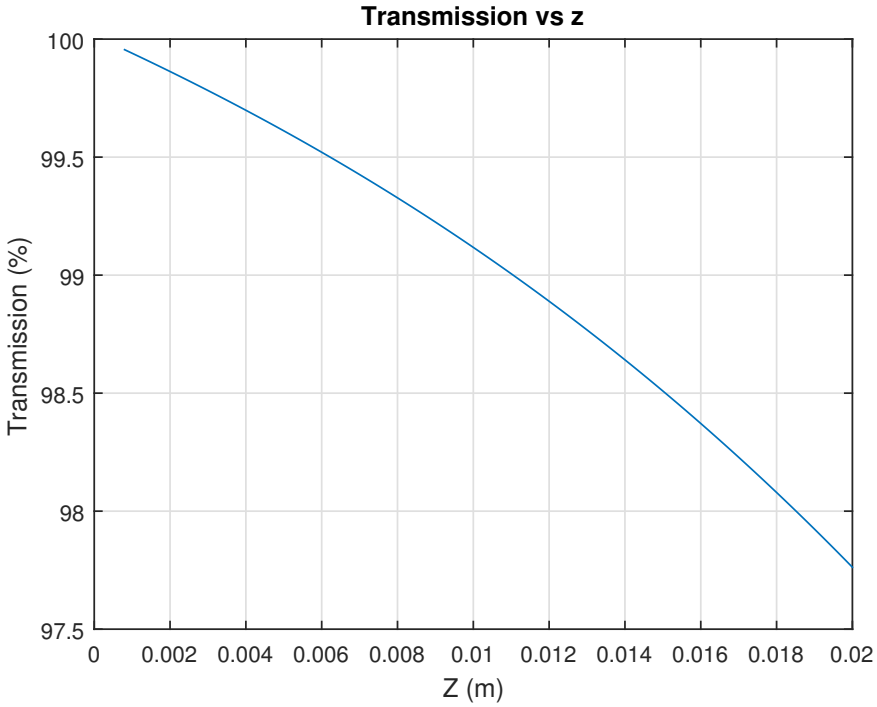

Figure 4.7: Simulation results of transmission vs atom-light interactions (measured in propagation distance)

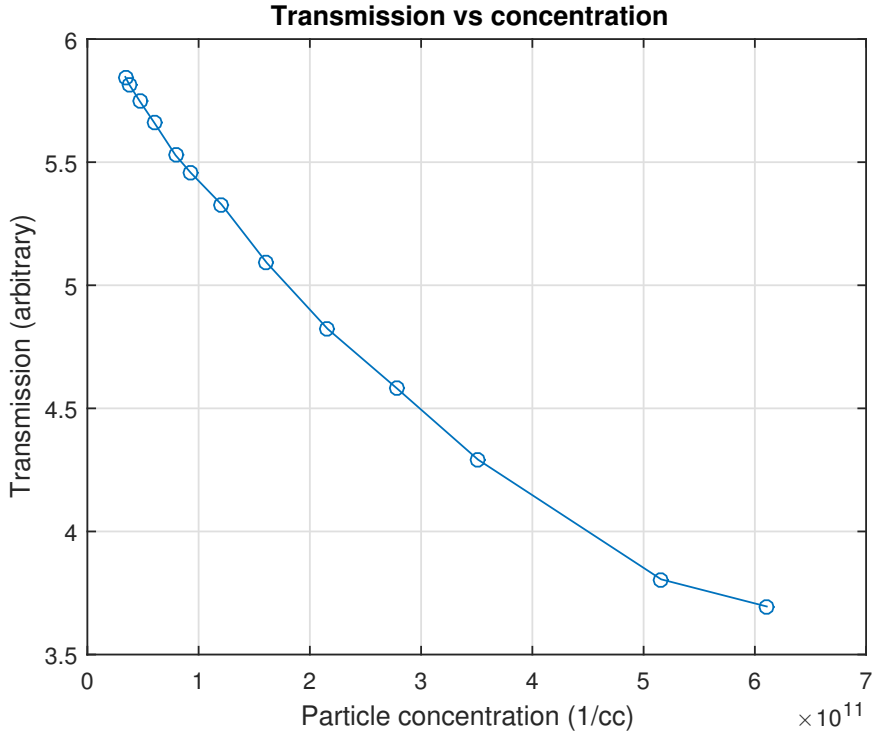

Figure 4.8: Experimental results of transmission vs atom-light interactions (measured in particle concentration). Power to the cell is 50 μW.

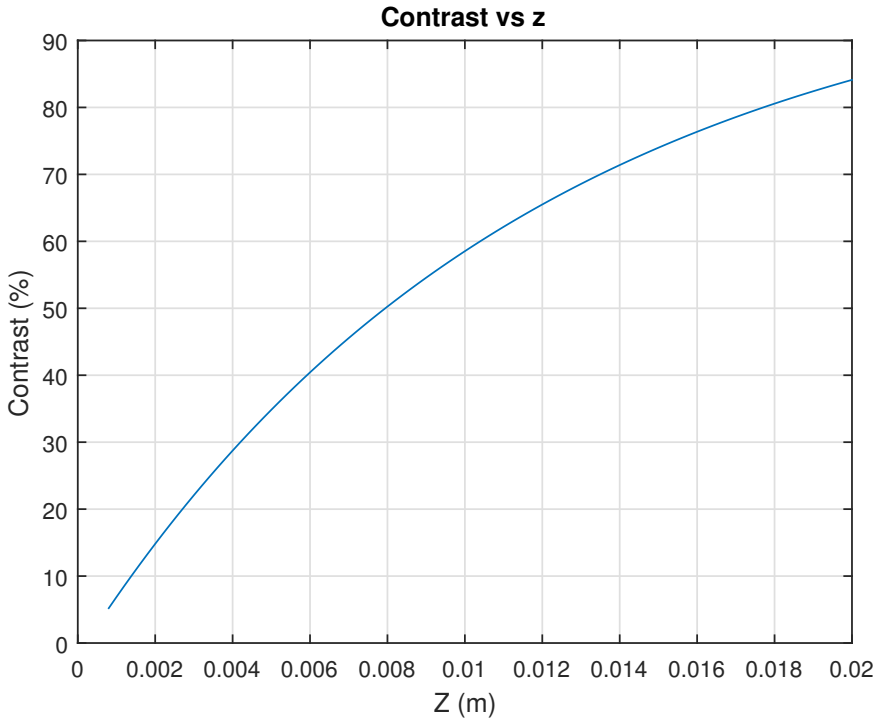

Figure 4.9: Simulation results of contrast vs atom-light interactions (measured in propagation distance)

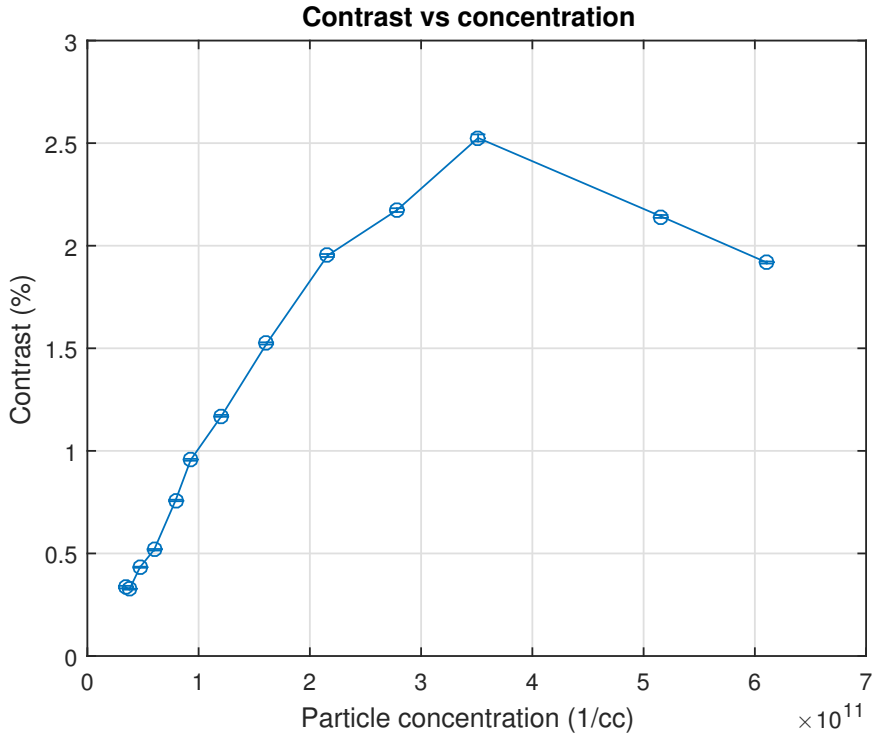

Figure 4.10: Experimental results of contrast vs atom-light interactions (measured in particle concentration) with a full beam. Power to the cell is 50 μW.

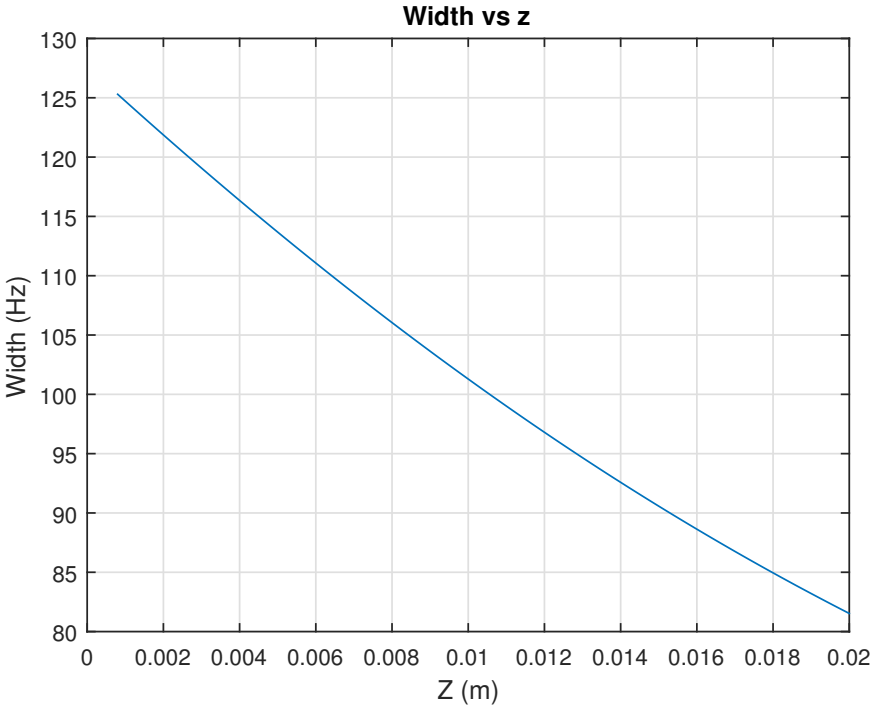

Figure 4.11: Simulation results of linewidth vs atom-light interactions (measured in propagation distance)

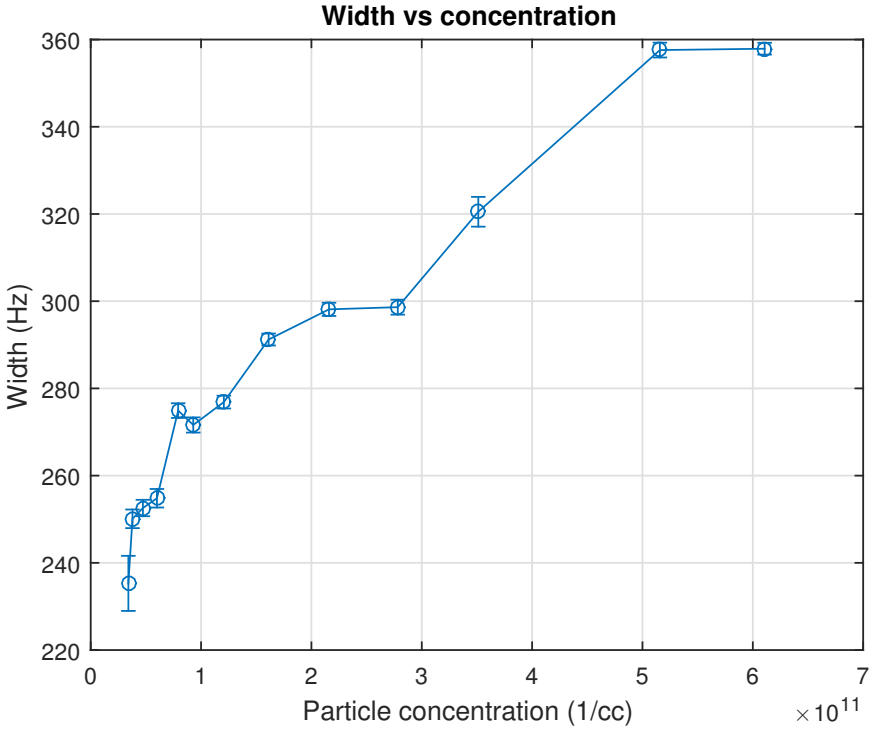

Figure 4.12: Experimental results of linewidth vs atom-light interactions (measured in particle concentration). Power to the cell is 50 μW.

Unlike our simulation results, however, here linewidth increases with concentration. This can be seen when comparing Figures 4.11 and 4.12. The increase in width is likely due to the ground state decay rate, γ_{bc}, truly being a function of concentration (n) and not a constant as it was in simulation. It is clear that we see significantly broader linewidths and smaller contrasts experimentally than in simulation. This is not surprising given that we are operating in a different regime of drive and (especially) probe Rabi frequency.

Figures 4.13 and 4.14 show summaries of experimental trends for contrast and linewidth, respectively.

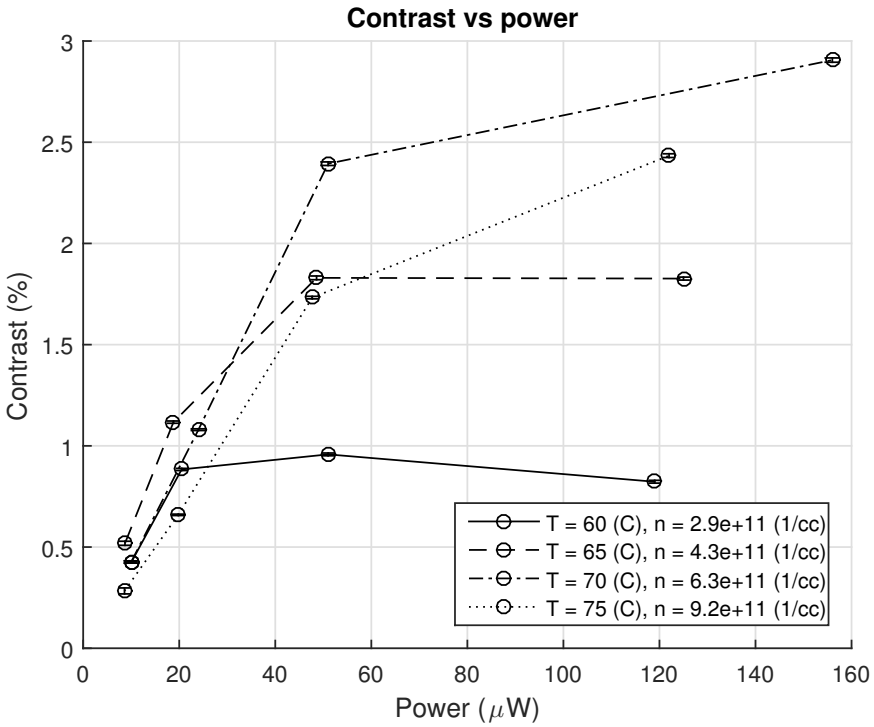

Figure 4.13: Contrast vs power for varying particle concentration with a beam waist of $1.2\omega_0$

4.2.2 Contrast and linewidth vs intensity for varying beam waist

Figures 4.15 and 4.16 show the data collected as detailed in Section 4.1.4. The x-axis of the plots was converted to a percentage of full intensity from the power measurements in order to show a better comparison of changes in waist size (which have comparable intensities, but

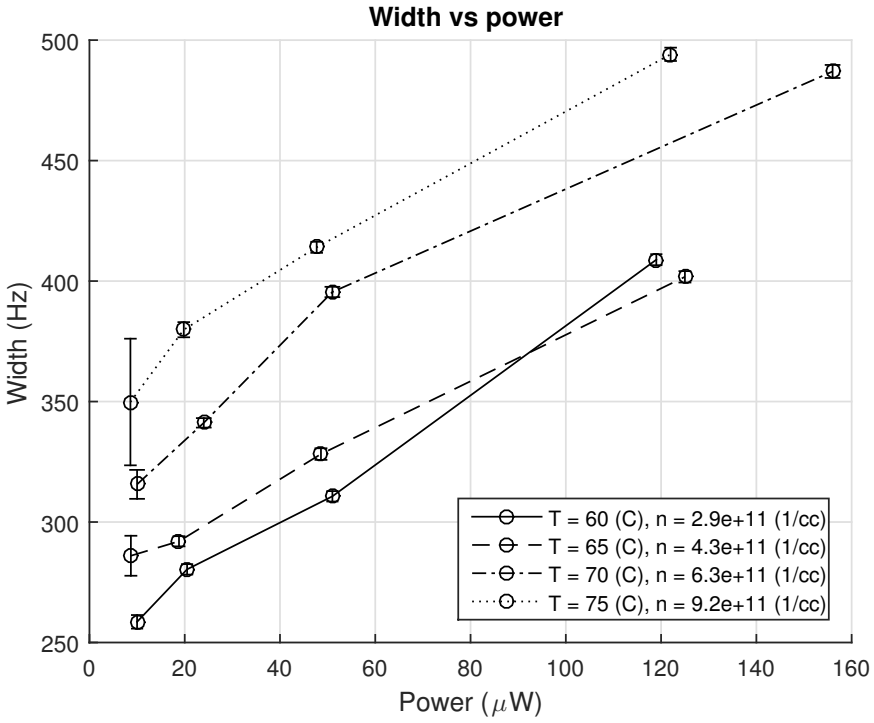

Figure 4.14: Linewidth vs power for varying particle concentration with a beam waist of $1.2\omega_0$

different total power). We see that contrast decreases with smaller waist sizes. By comparing Figure 4.15 with Figure 4.4, we can see that this is in the region where contrast decreases with power. The important observation here is in Figure 4.16, where it is evident that a smaller waist size results in a finer linewidth. This data contains the largest contrast observed of 3.9% with a linewidth of 657 Hz (used in Figure 3.2 as an example of the Lorentzian fit).

Shown in Figure 4.17, our narrowest linewidth of 202 Hz with a contrast of 0.84% was achieved with an iris set to allow 5% of total beam power to pass. This would correspond with a waist size of $0.3\omega_0$. The beam was attenuated to 20% intensity (actual power to the cell being 10 μW). Unfortunately, we found that the beam diffracted significantly at this iris setting, and so the data cannot be compared with the given trends of beam waist.

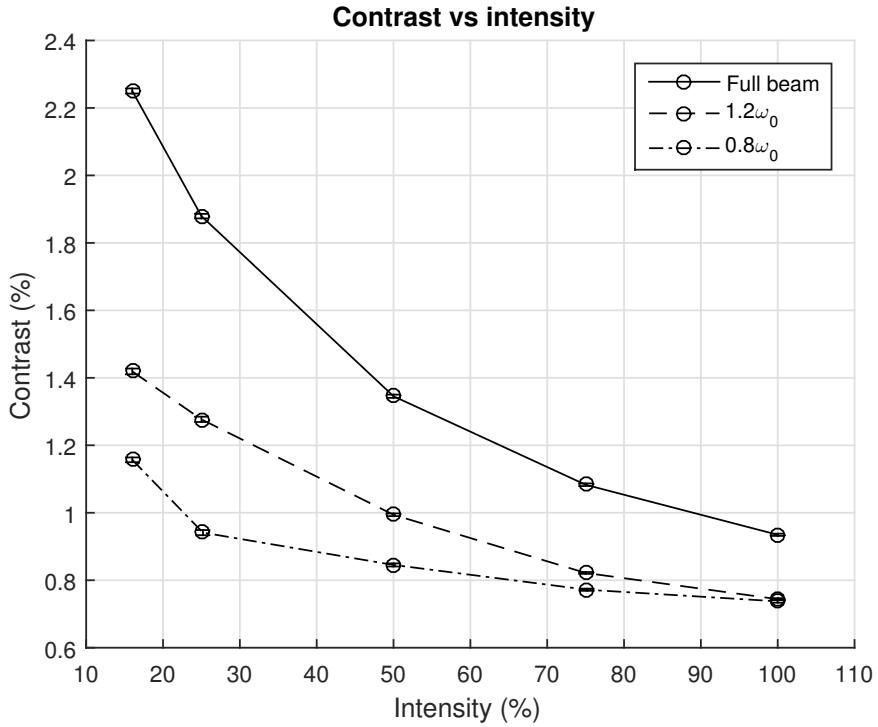

Figure 4.15: Contrast vs intensity for varying beam waist. Full power to the cell with a full beam is 1 mW.

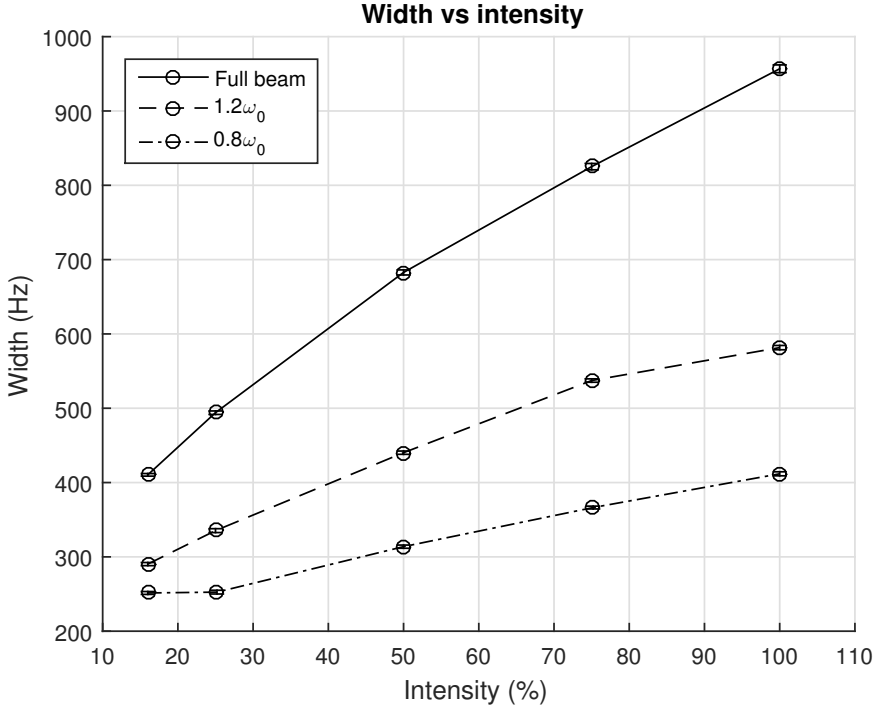

Figure 4.16: Width vs power for varying beam waist. Full power to the cell with a full beam is 1 mW.

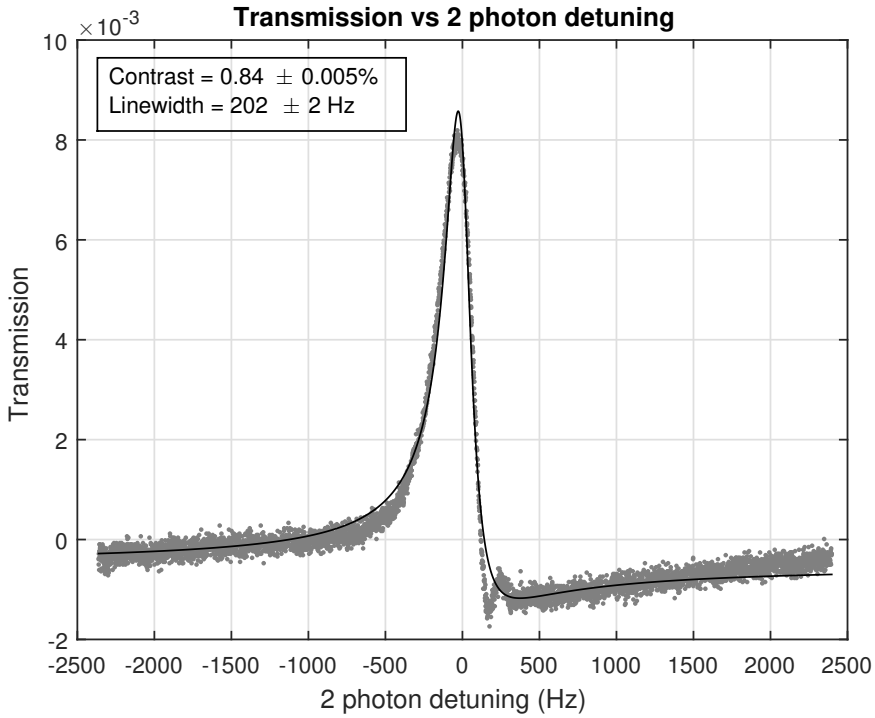

Figure 4.17: Fit of experimental EIT with a contrast of 0.84% and linewidth of 202 Hz. This is the narrowest linewidth observed experimentally.

4.3 Error analysis

We have encountered multiple noise and error sources which have impacted data collection. These have ranged from benign technical problems involving our heating element, to possibly data altering errors due to faults in electronics. We have identified one of these sources as the magnetic field generated by current through our heating element inside the magnetic shield. This magnetizes the shield and has had an affect of widening the resonance linewidths discussed in Section 4.2. We have also observed excessive noise in the data, though the source is not yet known.

As explained in Section 4.1.1, we have 3 fields. These fields are a drive and 2 sidebands, one of which acts as our probe. All 3 of these fields contribute to the transmission seen at the photodiode, and thus affect our contrast measurements. This means that given contrasts are smaller than actual probe contrasts by at least a factor of 2.

Conclusions

We have simulated EIT in 3 state atoms with properties based on those of ^{87}Rb. The drive Rabi frequency ranged from 16.6 to 25 kHz with a fixed probe Rabi frequency of 0.1 Hz. EIT with contrasts above 50% and linewidths of less than 100 Hz, suitable for use as a frequency filter, were found in simulation for media lengths of up to 2 cm. We have demonstrated EIT experimentally, though due to technical limitations both our drive and probe Rabi frequencies are several orders of magnitude higher than simulation parameters, ranging from approximately 5 to 30 MHz. Contrast and linewidth are determined by fitting the data to a generalized Lorentzian. The smallest linewidth observed is 202 Hz, with a contrast of 0.84%. The largest contrast observed is 3.9% with a linewidth of 657 Hz.

References

[1] H. J. Kimble, Yuri Levin, Andrey B. Matsko, Kip S. Thorne, and Sergey P. Vyatchanin. Conversion of conventional gravitational-wave interferometers into quantum nondemolition interferometers by modifying their input and/or output optics. *Phys. Rev. D*, 65:022002, Dec 2001.

[2] Eugeniy E. Mikhailov, Keisuke Goda, Thomas Corbitt, and Nergis Mavalvala. Frequency-dependent squeeze-amplitude attenuation and squeeze-angle rotation by electromagnetically induced transparency for gravitational-wave interferometers. *Phys. Rev. A*, 73:053810, May 2006.

[3] Nathan Belcher, Eugeniy E. Mikhailov, and Irina Novikova. Atomic clocks and coherent population trapping: Experiments for undergraduate laboratories. *American Journal of Physics*, 77(11):988–998, 2009.

[4] Eugeniy Mikhailov. Nonlinear properties of dense coherent media. 2003.

[5] S. Knappe, M. Stähler, C. Affolderbach, A.V. Taichenachev, V.I. Yudin, and R. Wynands. Simple parameterization of dark-resonance line shapes. *Applied Physics B*, 76(1):57–63.

[6] Daniel A Steck. Rubidium 87 d line data, 2001.

[7] M. Klein, M. Hohensee, D. F. Phillips, and R. L. Walsworth. Electromagnetically induced transparency in paraffin-coated vapor cells. *Phys. Rev. A*, 83:013826, Jan 2011.